Molecular Cell, Volume *65*

Supplemental Information

Identification of an RNA Polymerase III Regulator Linked to Disease-Associated Protein Aggregation

Olga Sin, Tristan de Jong, Alejandro Mata-Cabana, Michelle Kudron, Mohamad Amr Zaini, Francesco A. Aprile, Renée I. Seinstra, Esther Stroo, Roméo Willinge Prins, Céline N. Martineau, Hai Hui Wang, Wytse Hogewerf, Anne Steinhof, Erich E. Wanker, Michele Vendruscolo, Cornelis F. Calkhoven, Valerie Reinke, Victor Guryev, and Ellen A.A. Nollen

A

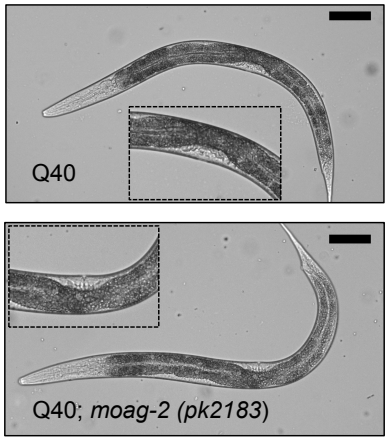

B

Reference	Variants	Gene	Amino Acid Change	Type of Mutation
C	T	*tag-124*	Ser89Phe	missense
C	T	*R05H5.4*	Gly155Arg	missense
C	T	*R166.3*	Asp50Asn	missense
C	T	*col-80*	Pro160Ser	missense
C	**T**	***lir-3***	**Met1Ile**	**loss of start codon**
C	T	*npp-3*	Ala1336Thr	missense

C

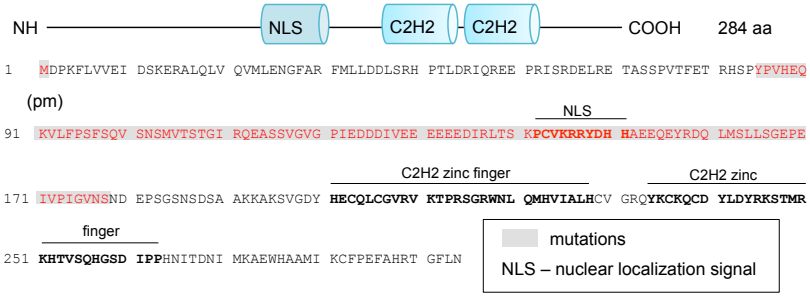

D

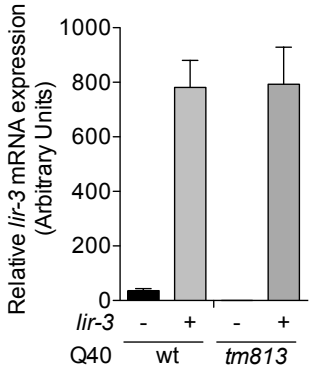

E

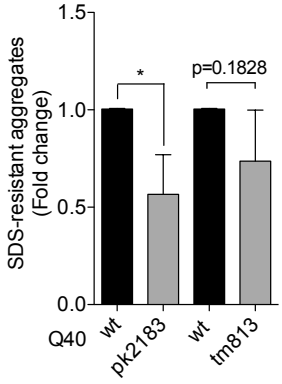

A

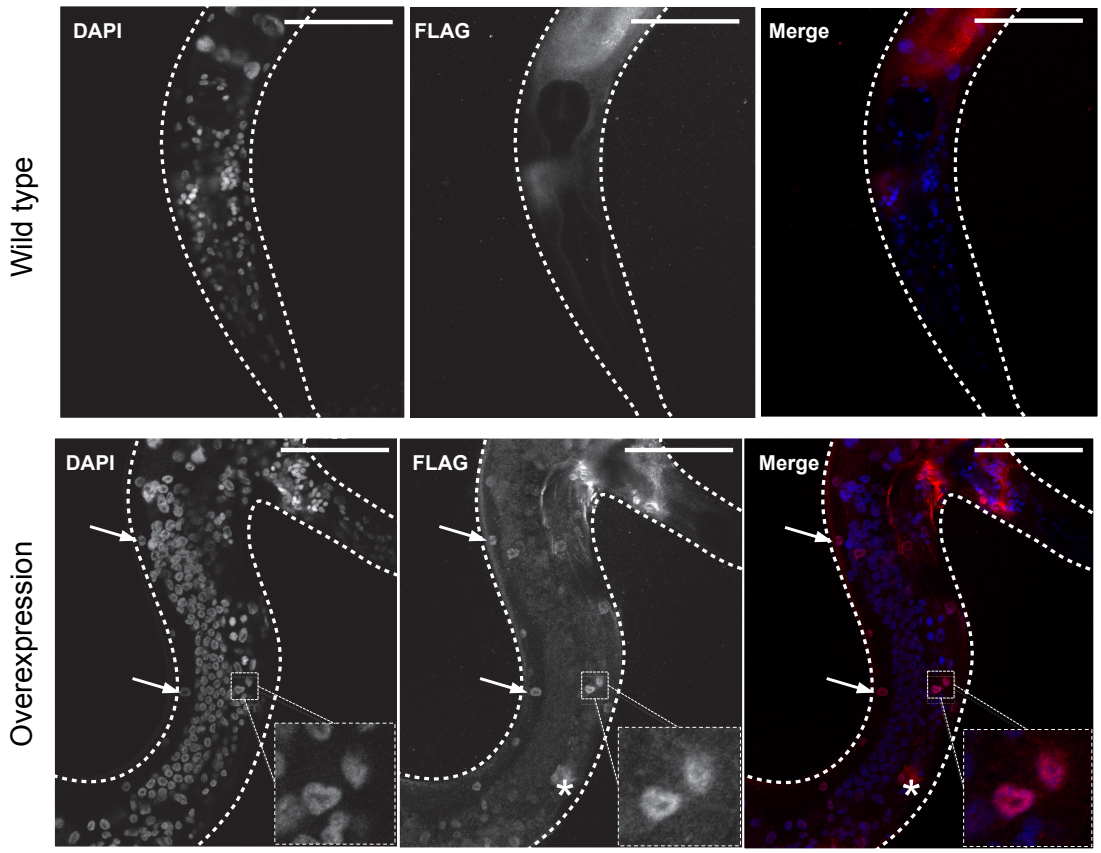

B

	MOAG-2/LIR-3 ChIP seq			Whole genome	
	Absolute	Relative (%)	P value	Absolute	Relative (%)
Protein coding	121	14.9	ns	20377	44.8
Pseudogene	13	1.6	ns	1431	3.1
ncRNA	300	36.9	ns	22753	50.1
rRNA	20	2.5	<0.001	20	0
snlRNA	0	0	ns	4	0
snoRNA	51	6.3	<0.001	139	0.3
snRNA	18	2.2	<0.002	114	0.3
tRNA	290	35.7	<0.001	609	1.3
Total	813	100		45447	100

A

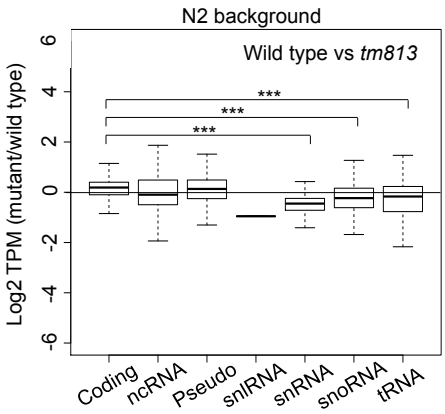

B

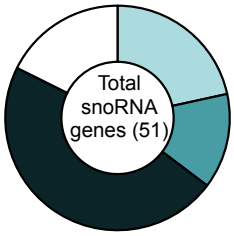

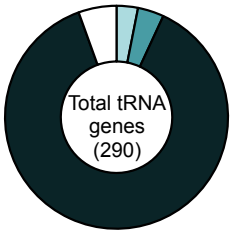

Box A (11)
Box B (7)
Box A and Box B (24)
Neither (9)

Box A (9)
Box B (11)
Box A and Box B (254)
Neither (16)

C

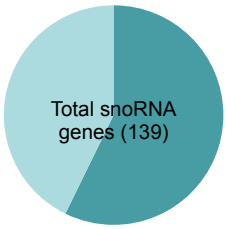

Genome
Pol II transcribed (79)
Pol III transcribed (59)

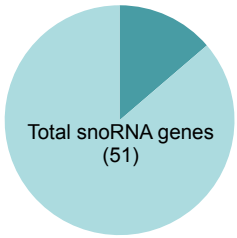

ChIP Seq
Pol II transcribed (7)
Pol III transcribed (44)

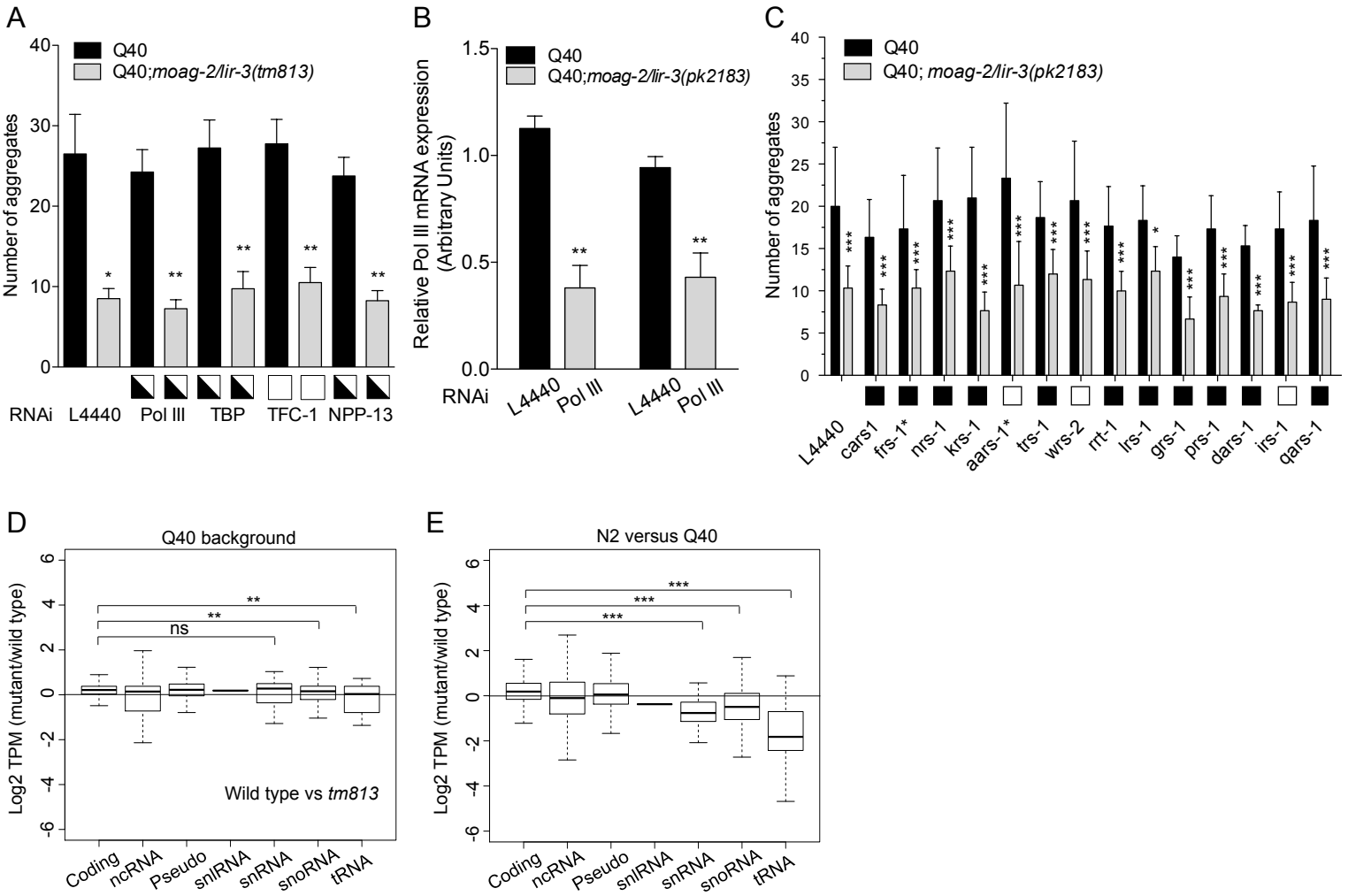
A
Q40
Q40;moag-2/lir-3(tm813)
Number of aggregates
RNAi L4440 Pol III TBP TFC-1 NPP-13
B
Q40
Q40;moag-2/lir-3(pk2183)
Relative Pol III mRNA expression (Arbitrary Units)
RNAi L4440 Pol III L4440 Pol III
C
Q40
Q40; moag-2/lir-3(pk2183)
Number of aggregates
L4440 cars-1 frs-1* nrs-1 krs-1 aars-1* trs-1 wrs-2 rrt-1 lrs-1 grs-1 prs-1 dars-1 irs-1 qars-1
D
Q40 background
Log2 TPM (mutant/wild type)
ns
Wild type vs tm813
Coding ncRNA Pseudo snlRNA snRNA snoRNA tRNA
E
N2 versus Q40
Log2 TPM (mutant/wild type)
Coding ncRNA Pseudo snlRNA snRNA snoRNA tRNA

A

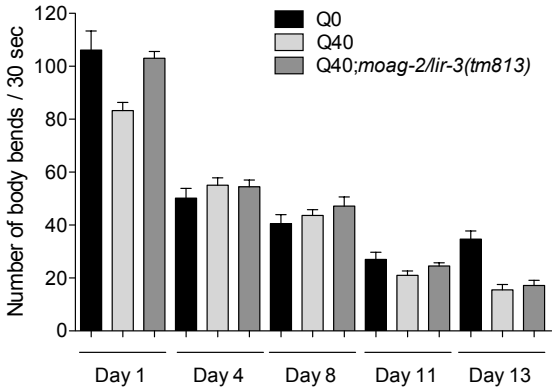

B

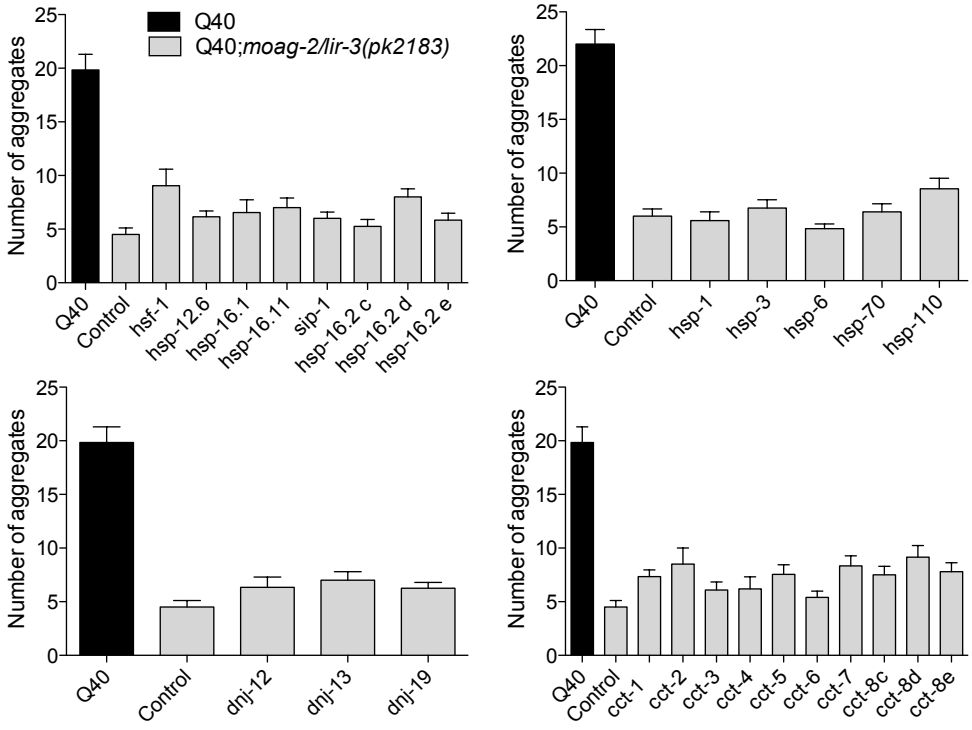

C

% Ratio Cytosol/Input			Fold change
	OE	Q40;OE	
Replicate 1	13.08	56.26	4.30
Replicate 2	4.26	71.35	16.74
Replicate 3	4.52	14.35	3.17

SUPPLEMENTAL FIGURE LEGENDS

Figure S1. Identification of *moag-2* as *lir-3* (related to Figure 1).
(A) Representative bright field images of L4-staged Q40 and Q40;*moag-2(pk2183)* worms. Insets show a magnification of the vulva. Scale bar, 75 μm.
(B) List of candidate genes for *moag-2* obtained by whole genome sequencing.
(C) Amino acid sequence of LIR-3 with the predicted nuclear localization signal (NLS, residues 132-141) and C2H2 zinc finger domains (residues 191-214 and 224-247). Grey shadow indicates location of the point mutation (pm) and the deleted residues in the *lir-3(tm813)* mutant.
(D) Transcript levels of *moag-2/lir-3* measured by quantitative PCR in Q40 and Q40;*lir-3(tm813)* worms from Figure 1E.
(E) Quantification of filter retardation assays by densitometry using ImageJ. The average of three biological replicates is represented. Data are represented as mean ± SEM and significance was calculated using a one-tailed unpaired Student's t-test. *$p<0.05$

Figure S2. Characterization of MOAG-2/LIR-3 as a nuclear protein that binds to the promoters of small ncRNAs (related to Figure 2).
(A) Subcellular localization of MOAG-2/LIR-3 in wild type N2 worms or worms overexpressing MOAG-2/LIR-3. Scale bar, 50 μm. Arrowheads point at nuclei; asterisks indicate non-specific staining.
(B) Number of MOAG-2/LIR-3 binding sites per gene biotype and total number of known *C. elegans* genes. The p values were calculated by permutation test.

Figure S3. MOAG-2/LIR-3 as a transcriptional regulator of small ncRNAs (related to Figure 3).
(A) Boxplot showing the relative expression of different gene biotypes in *lir-3(tm813)* relative to the wild type N2 background. Coding: protein-coding genes; ncRNA: non-coding RNA; Pseudo: pseudogenes; snRNA: small nuclear RNA; snlRNA: snRNA-like RNA; snoRNA: small nucleolar RNA; tRNA: transfer RNA. The average of three biological replicates is represented. ***$p<0.001$
(B) Number of MOAG-2/LIR-3 binding sites containing Box A and Box B in snoRNA and tRNA genes.
(C) Number of snoRNA genes encoded by Pol II or Pol III genome-wide and detected in this study.

Figure S4. Excluding the involvement of RNA homeostasis in polyglutamine-induced aggregation (related to Figure 4).
(A) Number of aggregates measured upon RNAi knockdown of individual components of the Pol III complex in Q40 and Q40;*moag-2lir-3(tm813)* worms.
(B) Transcript levels of Pol III measured by quantitative PCR in Q40 and Q40;*moag-2/lir-3(pk2183)* worms from Figure 4A.
(C) Number of aggregates measured upon knockdown of tRNA synthetases in Q40 and Q40;*moag-2/lir-3(pk2183)* worms. Asterisks indicate genes previously known to reduce protein aggregation. In panels A and C, an internal quality control for RNAi was performed and squares indicate penetrance (100% [closed]; 50% [half-open] and 0% [open]) of all associated visible RNAi phenotypes other

than aggregation. Aggregate counting was performed at the L4 stage. Data are represented as mean ± SEM and significance was calculated using a two-tailed unpaired Student's t-test.
(D-E) Boxplot showing the relative expression of different gene biotypes in Q40 and Q40;*moag-2/lir-3(tm813)* worms **(D)** and in N2 and Q40 wild type worms (Q40 wild type outcrossed from *tm813*) **(E)**. Coding: protein-coding genes; ncRNA: non-coding RNA; Pseudo: pseudogenes; snRNA: small nuclear RNA; snlRNA: snRNA-like RNA; snoRNA: small nucleolar RNA; tRNA: transfer RNA. *p<0.05; **p<0.01; ***p<0.001; ns is not significant. In all panels, the average of three biological replicates is represented.

Figure S5. Polyglutamine moves MOAG-2/LIR-3 to the cytosol where it turns into a positive regulator of protein aggregation (related to Figure 5).
(A) Number of body bends in Q0, Q40 wild type and Q40 worms overexpressing MOAG-2/LIR-3 (Q40;OE). One biological replicate is represented.
(B) Number of aggregates represented as fold change measured upon RNAi knockdown of cellular folding factors in Q40;*moag-2/lir-3(pk2183)* worms.
Aggregate counting was performed at the L4 stage and one representative experiment of three biological replicates is represented. Data are represented as mean ± SEM and significance was calculated using One-way ANOVA. ***p<0.001
(B) Quantification of the fraction of MOAG-2/LIR-3 present in the cytosol. The intensity of the bands was quantified using ImageJ. The FLAG signal in the input and cytosol were normalized against the signal for α-tubulin.

SUPPLEMENTAL TABLES

Table S1. Strains used in this study (related to Figures 1-5).

Strain name	Genotype	Source
N2 (Bristol)	wild type	
AM141	rmIs133[P(unc-54)Q40::YFP]X	Morley et al., 2002
OW1019	moag-2 (pk2183)	
OW1002	lir-3(tm0813)II	
OP312	wgIs312[P(lir-3)::TY1::EGFP::3xFLAG + unc-119(+)]	Sarov et al., 2006; Zhong et al., 2010
OW1009	mIs[P(unc-54)::Q0::YFP]V	
OW1021	rmIs133[P(unc-54)Q40::YFP]X	
OW1020	rmIs133[P(unc-54)Q40::YFP]X;moag-2(pk2183)II	
OW1004	rmIs133[P(unc-54)Q40::YFP]X	
OW1046	rmIs133[P(unc-54)::Q40::YFP]X; lir-3(het)II	
OW1003	rmIs133[P(unc-54)Q40::YFP]X;lir-3(tm813)II	
OW1096	rmIs133[P(unc-54)::Q40::YFP]X; zgEx221[P(myo-3)::CFP]	
OW1097	rmIs133[P(unc-54)::Q40::YFP]X; zgEx221[P(myo-3)::CFP]; lir-3(tm813)II	
OW1094	rmIs133[P(unc-54)::Q40::YFP]X; zgEx226[P(myo-3)::CFP + P(lir-3)::lir-3]	
OW1095	rmIs133[P(unc-54)::Q40::YFP]X; zgEx226[P(myo-3)::CFP + P(lir-3)::lir-3]; lir-3(tm813)II	
OW1059	rmIs133[P(unc-54)::Q40::YFP]X;[P(lir-3)::GFP::3xFLAG]	

Table S2. Overview and statistical analysis of aggregate counting experiments (related to Figure 1, 4, S4 and S5).
This table includes raw data showing the average number of aggregates and p values for the panel(s) in Figures 1, 4, S4 and S5.

Table S3. Analysis of differential expression between Q40 and Q40;*moag-2/lir-3* mutants (related to Figure 4 and S4).
This table includes raw data showing the changes in transcription between Q40 and Q40;*moag-2/lir-3* mutants in Figure 4 and S4).

Supplemental References

Morley, J.F., Brignull, H.R., Weyers, J.J., and Morimoto, R.I. (2002). The threshold for polyglutamine-expansion protein aggregation and cellular toxicity is dynamic and influenced by aging in Caenorhabditis elegans. Proc. Natl. Acad. Sci. USA *99*, 10417–10422.

Sarov, M., Schneider, S., Pozniakovski, A., Roguev, A., Ernst, S., Zhang, Y., Hyman, A.A., and Stewart, A.F. (2006). A recombineering pipeline for functional genomics applied to Caenorhabditis elegans. Nat. Methods *3*, 839–844.